https://doi.org/10.5194/egusphere-2025-1924
Preprint. Discussion started: 19 May 2025
© Author(s) 2025. CC BY 4.0 License.

Constraining the time of emergence of anthropogenic signal in the global land carbon sink

Na Li[1, 2], Sebastian Sippel[2], Nora Linscheid[1, 3], Miguel D. Mahecha[3], Markus Reichstein[1], and Ana Bastos[1, 3]

[1]Max Planck Institute for Biogeochemistry, 07745 Jena, Germany.
[2]Institute for Meteorology, Leipzig University, 04103 Leipzig, Germany.
[3]Institute for Earth System Science and Remote Sensing, Leipzig University, 04103 Leipzig, Germany.
[*]Address correspondence to: na.li@uni-leipzig.de

Abstract. The global land carbon sink has increased since the preindustrial period, driven by increasing atmospheric CO_2 concentration and climate change. However, detecting these anthropogenic signals in the global land carbon sink is challenging due to the large year–to–year variability, which can mask or amplify long-term trends, particularly on regional and decadal scales. This study aims to detect the time it takes for long-term trends driven mostly by anthropogenic signal to dominate over natural variations, that is, the "time of emergence", in the land carbon sink.

For this, we use five large ensembles of historical simulations (1851–2014) and future scenarios (2016–2100) by Earth system models. Our results show that, firstly, the anthropogenic signal in the global net land carbon sink emerges from 26 to 66 years in the period 1960–2019 (relative to the natural variations in the period of 1930–1959), depending on the ESM considered. The time of emergence is considerably shorter for the two major gross carbon fluxes: 8–13 years for gross primary productivity and 6–10 years for total ecosystem respiration. Furthermore, we find that long-term trends of net land carbon sink on most regional scales take at least 20 years more to emerge, due to larger contributions from internal climate variability at smaller scales.

Secondly, future scenarios show delayed signal detection compared to historical trends, due to a slow-down of the increasing net land carbon sink in response to emission mitigation, compared to the higher natural variability.

Thirdly, we apply dynamical adjustment to filter out the year–to–year circulation induced variability in both the historical and future simulations. This approach allows to substantially shorten the detection time for the global net land carbon sink: between 34–39% for the historical period and 27–54% for the future simulations. This approach can, in principle, be applied to observational based datasets, thereby improving our ability to detect long-term trends on land carbon sink variability. Given that long-term trends are mostly associated with human impacts on the land carbon cycle, our proposed approach can offer valuable insights on the effectiveness of policy decisions and their implementation.

1 Introduction

The global land carbon sink has been increasing since the pre-industrial period (Friedlingstein et al., 2022; Ruehr et al., 2023), mainly driven by increasing atmospheric CO_2 and mid- to high-latitude warming caused by human activities (O'Sullivan et al.,

https://doi.org/10.5194/egusphere-2025-1924
Preprint. Discussion started: 19 May 2025
© Author(s) 2025. CC BY 4.0 License.

2022). Detecting such anthropogenic signals in observations of annual atmospheric CO_2 concentration remains challenging due to the large year–to–year natural variations, which can obscure or enhance long-term trends, especially at regional scales and for shorter periods (Deser et al., 2012b; Kay et al., 2015; Maher et al., 2019; Chen et al., 2021; Bonan et al., 2021).

The global net land carbon sink refers to the balance between carbon absorption through gross primary productivity (GPP, photosynthesis at large scale) and carbon release through total ecosystem respiration (TER), but also through fires and other disturbances (Canadell et al., 2021; Ciais et al., 2022). GPP and TER are directly driven by local climate variability, such as temperature, precipitation (Jung et al., 2017; Piao et al., 2020; Canadell et al., 2021). Elevated atmospheric CO_2 concentrations have contributed to an increase in the global land carbon sink (Ruehr et al., 2023) through increasing GPP (Walker et al., 2021). Warming temperatures, particularly at high latitudes, have also contributed to increasing GPP (Ruehr et al., 2023).

The long-term trends in the global carbon cycle are superimposed by substantial year–to–year variations (Piao et al., 2020). These variations mostly stem from natural processes such as internal climate variability, variability on a continuum of time scales unrelated to external effects, as well as from influences from natural forcing such as volcanic eruptions and solar radiation (Deser et al., 2012b; Canadell et al., 2021; Eyring et al., 2021; Mercado et al., 2009; Zhang et al., 2021). Internal climate variability is often referred to as an irreducible noise in the signal of long-term forced climatic trends, and arises from internal atmospheric dynamics and interactions between the atmosphere and oceans (Deser et al., 2012a, 2020; Lehner et al., 2017; Bonan et al., 2021). Internal climate variability emerges as short-term weather events and long-term low-frequency climate variability patterns like El Niño/Southern Oscillation (ENSO) which are known to influenced global land carbon sink variations through local changes in temperature and precipitation (Bacastow, 1976; Keeling et al., 1995; IPCC, 2021; Li et al., 2022).

The detection of anthropogenic signals in the global land carbon sink is important for improving our understanding of carbon-climate feedback and refining future carbon projections (Friedlingstein et al., 2014). Detection involves identifying a statistically significant "signal" of long-term forced changes against the "noise" of natural variability in the system (Chen et al., 2021) and is important for improving our understanding of carbon-climate feedback and refining future carbon projections (Friedlingstein et al., 2014). However, several fundamental challenges remain:

First, internal climate variability can differ substantially, which may be seen as random and difficult to predict (Frankcombe et al., 2015; Deser et al., 2020; Doblas-Reyes et al., 2021; Bonan et al., 2021). Since observations only represent one unique realization of internal climate variability, they are insufficient to characterize the full range of physically plausible internal climate variability. Moreover, internal climate variability is sensitive to the choice and length of the study period (Kumar et al., 2016; Doblas-Reyes et al., 2021), making it harder to separate natural fluctuations from forced signals (Bonan et al., 2021; Frankcombe et al., 2015; Doblas-Reyes et al., 2021). Short-term observational records may not capture the full dynamics of internal climate variability (Maher et al., 2019; Chen et al., 2021).

Second, ecosystem responses vary across geographic regions and timescales of natural climate variations and forcing (Lombardozzi et al., 2014). Regions with high natural climate variability might not show high land carbon sink variability (Lombardozzi et al., 2014). The detection and attribution of anthropogenic signals thus strongly depend on the specific regions of interest (Deser et al., 2012b; Hawkins and Sutton, 2012; Deser et al., 2012a; Mahlstein et al., 2012; Lombardozzi et al., 2014).

https://doi.org/10.5194/egusphere-2025-1924
Preprint. Discussion started: 19 May 2025
© Author(s) 2025. CC BY 4.0 License.

On decadal time scales, internal climate variability in land-atmosphere CO_2 flux often mask the anthropogenic signals in many regions (Lombardozzi et al., 2014; Kumar et al., 2016; Doblas-Reyes et al., 2021; Bonan et al., 2021).

Large ensembles of Earth System Model (ESM) simulations with perturbed initial conditions are effective tools to address these challenges (Deser et al., 2020; Bonan et al., 2021). By running sufficient simulations in a single model with slightly different initial conditions, and under the same physical process representation and external forcing, the distribution of internal climate variability is sampled much better than in a single realization (Milinski et al., 2020; Chen et al., 2021). The externally perturbed signal (anthropogenic signal) emerges as the ensemble mean, that is, a deterministic signal. The residual after removing the ensemble mean can thus be regarded as mostly internal natural variability in the climate system (Milinski et al., 2020; Deser et al., 2020; Bonan et al., 2021). Based on such large ensembles of ESM simulations, the "time of emergence (ToE)" can be determined as the time required for an external perturbed signal (anthropogenic-caused climate change) to become larger than the amplitude of natural variations (Lehner et al., 2017; Bonan et al., 2021). The ToE metric helps to identify climate change impacts on regional and global scales, and attribute changes to particular causes (Chen et al., 2021). However, due to large year–to–year variations, the anthropogenic signal may remain within the range of natural variability for multiple decades (Lombardozzi et al., 2014; Bonan et al., 2021; Ranasinghe et al., 2021).

Here, we evaluate how long long-term trends in the global land carbon sink, mostly driven by anthropogenic perturbations need to be detected from local to global scales, by estimating the ToE in ESM simulations under historical and future scenarios. Our key objectives are to: 1) detect the anthropogenic perturbed signal in global land carbon sink in historical simulations (1851-2014); 2) examine the spatial effects in the ToE on regional scales; 3) estimate the ToE under various future scenarios (2016-2100) and 4) test approaches to separate circulation induced variability in the ToE in the global land carbon sink.

2 Methods and dataset

In this study, we use five ESM large ensembles to investigate the time to detect anthropogenic perturbed signals in global and regional land carbon sinks.

2.1 Dataset

We use outputs from historical simulations by ESMs with at least 30 realizations to investigate the ToE in the land carbon sink. The models selected include the CESM2-LE (Danabasoglu et al., 2020; Rodgers et al., 2021) and four models in CMIP6 (Eyring et al., 2016; Brunner et al., 2020): ACCESS-ESM1-5 (Ziehn et al., 2020), CanESM5 (Swart et al., 2019), IPSL-CM6A-LR (Boucher et al., 2020), and MPI-ESM1-2-LR (Mauritsen et al., 2019). All historical simulations are conducted under the CMIP6 historical forcing, including volcanic eruptions and changes in atmospheric composition due to human activities (Eyring et al., 2016).

The historical simulations covers the period of 1851-2014 and the future scenario simulations cover the period from 2015 to 2100. The spatial resolution of CESM2-LE outputs is $0.9375° \times 1.25°$, and four CMIP6 models is $2.5° \times 2.5°$ (pre-processed by Brunner et al. (2020) from their native spatial resolution). We select the net biome production (NBP), gross primary production

https://doi.org/10.5194/egusphere-2025-1924
Preprint. Discussion started: 19 May 2025
© Author(s) 2025. CC BY 4.0 License.

(GPP), and total ecosystem respiration (TER) from the above five Earth system models. Note that the TER in CESM2-LE is calculated according to Eq. (1), where TER is estimated as the difference between GPP, primary production (NPP), corresponding to autotrophic respiration, soil respiration (SR), and litter respiration (LR) (Eq. (1)).

$$TER = GPP - NPP + SR + LR \tag{1}$$

The TER in four CMIP6 models is calculated based on the sum of autotrophic (ra) and heterotrophic respiration (rh) (Eq. (2)).

$$TER = ra + rh \tag{2}$$

CESM2-LE outputs of NBP, GPP, NPP, SR, and LR are downloaded from https://www.earthsystemgrid.org/dataset/ucar.cgd.cesm2le.lnd.proc.monthly_ave.html, last accessed on July 11, 2024. For the other four CMIP6 models, NBP, GPP, ra and rh are downloaded (originally from https://esgf-node.llnl.gov/projects/cmip6/) then pretreated by Brunner et al. (2020), last accessed on July 11, 2024. We further download the monthly mean sea level pressure (SLP) from the five models from their respective sources.

For the regional analysis, we use the regional carbon cycle assessment and processes (RECCAP-2) (Ciais et al., 2022) map (https://www.bgc-jena.mpg.de/geodb/projects/Data.php) that categorizes the global land surface into10distinct domains, with resolution of $0.5° \times 0.5°$.

The future scenario simulations are modeled under different Shared Socioeconomic Pathways (SSPs) for the period 2015-2100, based on varying levels of human-emitted CO_2 and mitigation efforts (Chen et al., 2021; Lee et al., 2021; O'Neill et al., 2016):

1. SSP1-2.6, CO_2 emissions decrease and reach net zero by 2050. Global surface air temperature averaged over 2081-2100 is 0.5°-1.5° higher than in 1995-2014 (Chen et al., 2021; Lee et al., 2021; O'Neill et al., 2016).

2. SSP2-4.5, CO_2 emissions remain steady until 2050, with global surface air temperature averaged over 2081-2100 is 1.2°-2.6° higher than in 1995-2014 (Chen et al., 2021; Lee et al., 2021; O'Neill et al., 2016).

3. SSP3-7.0, without additional climate policies, CO_2 emissions doubled by 2100, leading to the global surface air temperature averaged over 2081-2100 increase of 2.0°-3.7 ° relative to 1995-2014 (Chen et al., 2021; Lee et al., 2021; O'Neill et al., 2016).

4. SSP5-8.5 Without additional climate policies, CO_2 emissions doubled by 2050, with global surface air temperature averaged over 2081-2100 rising by 2.4°-4.8° relative to 1995-2014 (Chen et al., 2021; Lee et al., 2021; O'Neill et al., 2016).

https://doi.org/10.5194/egusphere-2025-1924
Preprint. Discussion started: 19 May 2025
© Author(s) 2025. CC BY 4.0 License.

2.2 Date pretreatment

NBP, GPP, and TER from CESM2-LE are provided in the unit of $gC \cdot m^{-2} \cdot s^{-1}$, from which an annual sum is calculated. NBP, GPP, and TER from four CMIP6 models are in unit of $kgC \cdot m^{-2} \cdot s^{-1}$ and converted to annual sums in $gC \cdot m^{-2} \cdot year^{-1}$. TER is calculated according to Eq. (1) for CESM2-LE and according to Eq. (2) in the four CMIP6 models. In order to have consistent sign with GPP, TER here is multiplied by –1. In the historical simulations (1851–2014), NBP, GPP, and TER of the five model datasets are area–weighted and aggregated to domain mean with the resolutions of 2.5°×2.5°, 5°×5°, 10°×10°, 20°×20°, 30°×30°, 45°×45°, 60°×60°, and global mean. The global mean of NBP, GPP, and TER is also calculated for the four future scenarios, with period of 2016–2100 selected (in CMIP6 models the time series starts at July 2015, so we select from 2016 instead). Note that CESM2-LE only includes one future scenario (SSP3-7.0). Sea level pressure from all five Earth system models is aggregated to the resolution of 10°×10°.

The RECCAP-2 map is area–weighted and aggregated to 2.5°×2.5°, then categorize the NBP, GPP, and TER to 10 RECCAP-2 regions.

2.3 Methods

2.3.1 Time of emergence

To determine the time of emergence (ToE), we apply the noise–to–signal ratio approach, following Bonan et al. (2021). The signal (S) refers to the anthropogenic perturbation driven response, which is given by the linear trend of the ensemble mean of the simulations for each model (Bonan et al., 2021). In the historical simulations, the noise (N) corresponds to the standard deviation of the ensemble before the 1950s, a period less affected by human activities compared to more recent ones, and used as the baseline for natural variability (Bonan et al., 2021). ToE (Eq. (3)) represents the time needed for the anthropogenic perturbed signal to become larger than the amplitude of the noise (Bonan et al., 2021).

$$ToE\ (years) = 2N/S \tag{3}$$

2.3.2 Noise filtering based on dynamical adjustment

To shorten the detection time, we use a dynamical adjustment technique to estimate circulation induced variability in NBP. Dynamical adjustment is a technique in climate science, which aims to isolate circulation induced variability (such as in temperature and precipitation); where the residual time series in those climate variables is thought to contain the forced response (Smoliak et al., 2015; Deser et al., 2016; Sippel et al., 2019). circulation induced variability is generally expected to reflect internal climate variability to the largest extent (Deser et al., 2016; Smoliak et al., 2015; Sippel et al., 2019). Therefore, dynamical adjustment allows to obtain a higher signal–to–noise ratio in the residual, that is circulation filtered, time series (the residual is the remainder after subtraction of the estimated circulation induced variability in a target variable).

https://doi.org/10.5194/egusphere-2025-1924
Preprint. Discussion started: 19 May 2025
© Author(s) 2025. CC BY 4.0 License.

Here, we employ ridge regression, a linear statistical learning technique, to estimate circulation induced-variability (Sippel et al., 2019). In our model, the sea level pressure (SLP) field is used as predictor and proxy of circulation induced variability to predict the circulation induced variability (Sippel et al., 2019). As a regularized linear regression, ridge regression allows for including full spatiotemporal dynamics of circulation variations while overcoming multicollinearity and overfitting, normally raising from a large number of predictors and relatively short study period (Hastie et al., 2009; Sippel et al., 2019). This approach was adapted by Li et al. (2022) to evaluate the fraction of atmospheric circulation induced variations in global carbon cycle variability. The key steps include (Sippel et al., 2019; Li et al., 2022): 1) Selecting pixel based time series of global SLP to predict global carbon cycle variability; here the full global domain. Then calculate the mean seasonal SLP. Since DJF (December, January, and February) SLP has the highest predictability of annual NBP (details please check Li et al. (2022)), here we select DJF SLP. 2) Selecting the time series to represent global carbon cycle variability as target variable; here, this corresponds to the global annual NBP with ensemble mean removed. 3) Splitting the dataset into training and testing groups; here, we select the first half period of the dataset as the training group and the second half as the testing group. For example in historical simulations, the training data is the time series from 1851 to 1932, and the testing data is in 1933–2014. 4) Switch the training and testing data to start a new round of model training and prediction. This means, the training data from step 3 is used as testing data, and the testing data from step 3 is used as training data. Then we have the full time series of NBP that is predicted by DJF SLP. Detailed model design can be found in Sippel et al. (2019); Li et al. (2022).

By using DJF SLP to predict NBP, we estimate the fraction of circulation induced variability in global NBP time series. The residual, after removing the DJF SLP predicted NBP, reflects mostly the influence of natural forcing (e.g., volcanic eruptions or solar radiation variability), disturbances (fires, when simulated by models), and unpredictable high frequency internal climate variability (Sippel et al., 2019; Piao et al., 2020; Canadell et al., 2021). We hypothesize that this method reduces noise levels in NBP and allows for an earlier detection of the anthropogenic signal.

2.4 Statistical analysis

We perform four statistical analyses: 1) ToE in land carbon fluxes from historical simulations: We analyse the time to detect anthropogenic perturbed signal in NBP, GPP, and TER in the historical simulations. Following Bonan et al. (2021), the signal (S) is the linear regression slope of the ensemble mean in the period of 1960–2009, and noise (N) is the standard deviation of all simulations in the period 1930–1959. We first compare the historical time series of NBP, GPP, and TER, and then calculate the ToE according to Eq. (3). 2) Spatial effects on ToE: We examine how the ToE varies globally and across 10 RECCAP-2 regions. Additionally, we evaluate the impact of spatial resolution on ToE by calculating pixel-based ToE at various scales (ranging from $2.5° \times 2.5°$ to $60° \times 60°$) and compare these with the global scale. 3) ToE in future projections of the land carbon fluxes: We calculate the ToE for NBP, GPP, and TER, with the signal period in 2020–2070 and the noise period in 2020–2050 (with the ensemble mean removed). 4) Noise reduction through dynamical adjustment: Given the large year–to–year variability in NBP, we use ridge regression to remove the circulation induced variability. To assess the effectiveness of ToE reduction through dynamical adjustment, we calculate the relative reduction (d_S) according to Eq. (4).

https://doi.org/10.5194/egusphere-2025-1924
Preprint. Discussion started: 19 May 2025
© Author(s) 2025. CC BY 4.0 License.

Note that only the calculated signal (regression slope) with significance value $P < 0.05$ is selected. If the calculated signal (regression slope) is negative, we then take the absolute signal value to get a positive ToE.

$$d_S = 100\% * (V_O - V_R)/V_O \tag{4}$$

Note that V_O represents the original value and V_R is the residual after the circulation induced variability estimated by the ridge regression model is removed.

3 Results and discussion

3.1 Detection of anthropogenic signal in historical simulations

We first examine the NBP time series for the historical simulations from 1851 to 2014 (Fig. 1). Before the 1960s, the ensemble mean (long-term trend) for each model remains relatively stable with slight variations. After the 1960s, the ensemble mean shows a noticeable increase. Despite this, the magnitude of NBP variability remains consistent or slightly increase throughout the historical period, for all models. In individual simulations, we observe that the year–to–year variations are considerably larger than the changes in the ensemble mean, enhancing or offsetting the long-term NBP trend.

We then examine the time series of GPP and TER in the historical simulations (Appendix A Fig.(A.1)). Both GPP and TER show similar trends across models, though ACCESS-ESM1-5 shows a larger magnitude difference. The ensemble mean of GPP and TER are similar until the 1960s, after which GPP slightly surpassed TER. Year–to–year variations are minor compared to the long-term trend in the ensemble mean, suggesting that photosynthesis and respiration are strongly influenced by anthropogenic perturbations. As GPP and TER trends compensate when combined to calculate NBP, NBP shows smaller long-term trends but significant year–to–year variability.

3.2 Spatial effects of ToE

We then examine how long it takes for the anthropogenic signal (ensemble mean of each model) to emerge from year–to–year variations of NBP in global scale and across 10 RECCAP-2 regions (Fig. 2). Globally, CESM2-LE has the shortest detection time at 26 years, while CanESM5 takes the longest at 66 years. ACCESS-ESM1-5 stands out with a much longer detection time of 289 years, due to a flat trend of ensemble mean after 1960s. Comparing noise (N) and signal (S) (Appendix A Fig. A.2 and Eq. (3)), we found that the variation in detection time across models is mainly due to differences in year–to–year variability.

In most of the 10 RECCAP-2 domains, ToE detection in NBP takes longer than at the global scale (Fig. 2B). The exception is ACCESS-ESM1-5, where a flat global trend after the 1960s causes a much longer detection time. The regional noise tends to be larger than at the global scale, leading to delayed detection of anthropogenic signals. We refer to this difference as "spatial delay". The spatial delay can be explained by reduced noise from internal climate variability when aggregating fluxes globally, while the signal remains relatively stable (Appendix A Fig. A.2). This is a well-known pattern in detection and emergence studies in the climate literature (Mahlstein et al., 2011; Lehner et al., 2017). Southeast Asia and Australasia, show

https://doi.org/10.5194/egusphere-2025-1924
Preprint. Discussion started: 19 May 2025
© Author(s) 2025. CC BY 4.0 License.

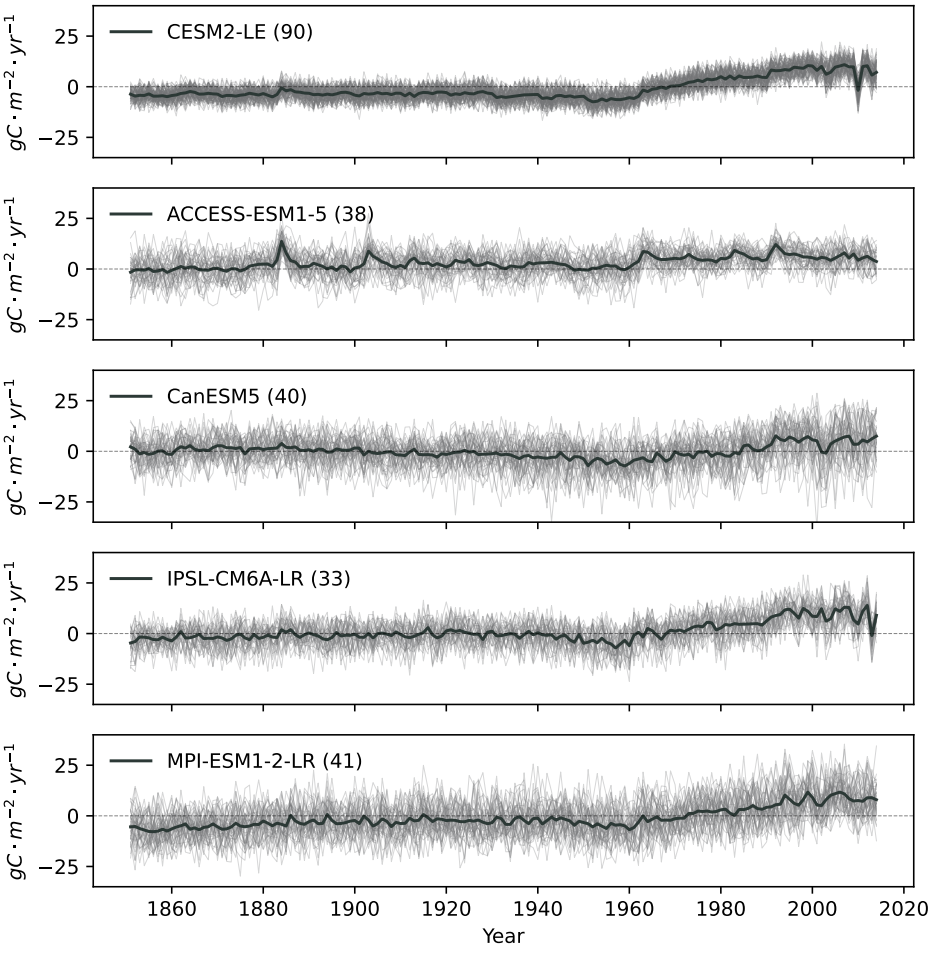

Figure 1. Time series of NBP from 1851 to 2014 in five ESM large ensembles. The thin lines represent individual simulations, while the bold lines represent the ensemble mean. The number of simulations for each model is listed in the legend next to the model name.

the largest noise, and therefore also the longest ToE across the 10 RECCAP-2 domains. However, the spatial delay does not apply everywhere. In Russia, models like ACCESS-ESM1-5, CanESM5, and IPSL-CM6A-LR show shorter detection time compared to the global scale. This is due to apparent smaller noise in Russia of the three models, compared with other regions and global scale Fig. A.2).

https://doi.org/10.5194/egusphere-2025-1924
Preprint. Discussion started: 19 May 2025
© Author(s) 2025. CC BY 4.0 License.

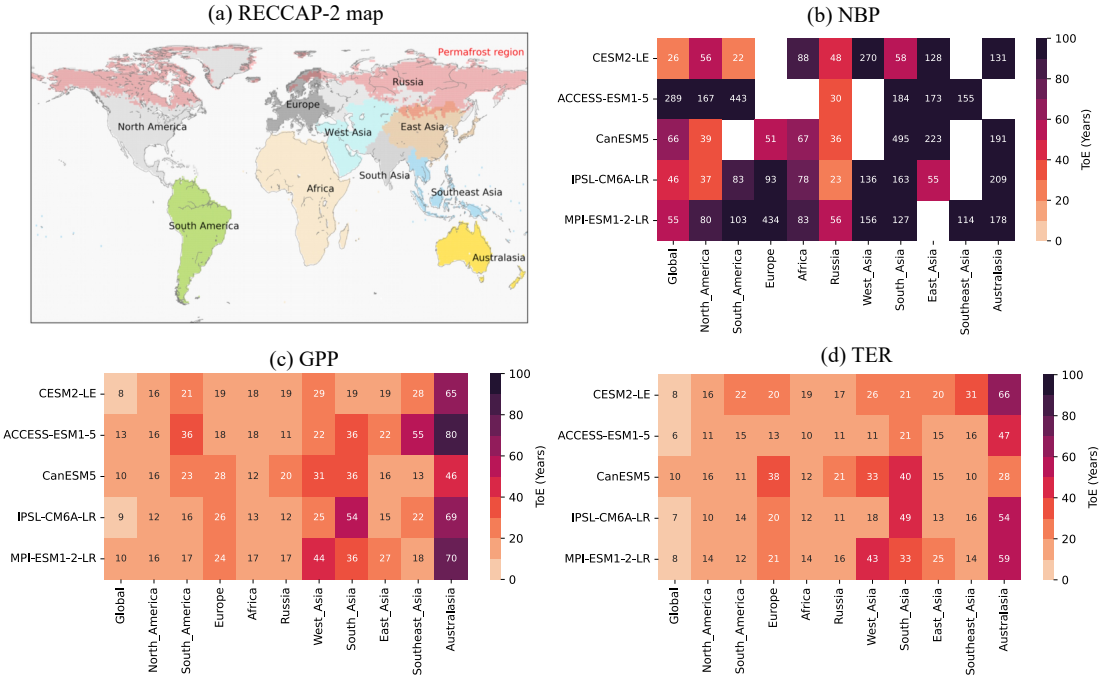

Figure 2. ToE of NBP on a global scale and across 10 RECCAP-2 regions, under historical simulations of five ESM large ensembles. Note that ToE is calculated with signal period of 1960-2009 relative to the noise period of 1930-1959, details please check Sect. 2.4. **(a)** RECCAP-2 map (duplicated from Ciais et al. (2022) Fig. 1) that divides the global continents into 10 domains. Note that the RECCAP-2 map is aggregated from $0.5^\circ \times 0.5^\circ$ to $2.5^\circ \times 2.5^\circ$, the spatial domains are slightly changed **(b)** Heat map of the ToE in global and each spatial domain of NBP. **(c)** and **(d)** are heat maps of the ToE in global and each spatial domain of GPP and TER separately. Domains with no significant signal ($P > 0.05$) are shown as empty squares.

We then evaluate the ToE for GPP and TER (Fig. 2C, D), which show similar patterns in detection time, and the relative importance of noise and signal at regional scale (Appendix A Fig. A.3, A.4). Globally, it takes around 8 to 13 years to detect anthropogenic signal in GPP and 6 to 10 years for TER. As found for NBP, both GPP and TER show a spatial delay from global scale to regional scale. Australasia in GPP and TER both have generally the longest detection time, due to high noise compared to low signal levels, indicating higher internal climate variability. In both GPP and TER, South America and Southeast Asia experience high level of noise and signal, while West Asia has relatively low level of noise and signal.

Compared with the land carbon sink (NBP), photosynthesis (GPP) and ecosystem respiration (TER) individually show a much shorter detection time of the anthropogenic signal (Fig. 2). This is likely due to the fact that GPP and TER trends are strongly influenced by anthropogenic perturbations, with the magnitude of the trend exceeding the magnitude of internal climate variability in a much shorter time. However, when calculating NBP, the long-term trends of GPP and TER offset each other, leaving NBP with weaker long-term trends relative to the year–to–year natural variations, thus making it harder to detect the anthropogenic signal in NBP.

https://doi.org/10.5194/egusphere-2025-1924
Preprint. Discussion started: 19 May 2025
© Author(s) 2025. CC BY 4.0 License.

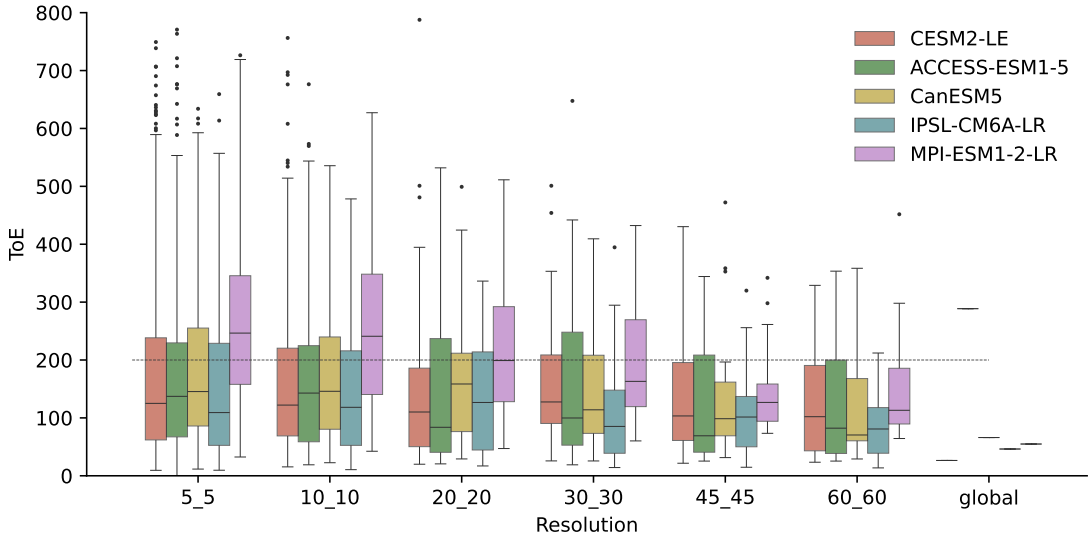

Figure 3. Spatial effect in NBP historical simulations across five ESM large ensembles. The distribution of ToE are shown for varying resolutions. Note that all the signals are in absolute values, so the calculated ToE are all positive.

To further analyse the spatial delay effect, we calculate the distribution of pixel based ToE for NBP, GPP, and TER under varying resolutions in the historical simulations. For NBP, as the resolution becomes coarser, the spread of the ToE distribution decreases substantially (Fig. 3), though the median remains similar. This supports the noise reduction by spatial aggregation through offsetting internal climate variability (Lombardozzi et al., 2014) (Fig. 3). A similar pattern is observed in GPP and TER, where aggregation reduces the spreads of ToE without substantially altering the medians (Appendix A Fig. A.5 and A.6).

We found that on a global scale, it takes shorter to detect long-term trends induced by anthropogenic effects than at smaller scales, with ToE increasing for smaller domains as reported by Lombardozzi et al. (2014), though their study used fewer models and less than 10 simulations. However, this spatial delay does not always apply, particularly in regions like Russia, the interannual natural variability in three CMIP6 models is apparently low compared with global scale.

In the historical simulations, the land carbon sink (NBP) shows large year–to–year variability, delaying the detection of anthropogenic signals. In contrast, GPP and TER are primarily driven by anthropogenic perturbations, with relatively lower natural variability. The compensating trends of TER and GPP delay NBP detection, explaining why GPP and TER detect the signal in around 10 years, while NBP takes around 26 to 66 years. Next, we explore how the different future climate scenarios impact ToE.

https://doi.org/10.5194/egusphere-2025-1924
Preprint. Discussion started: 19 May 2025
© Author(s) 2025. CC BY 4.0 License.

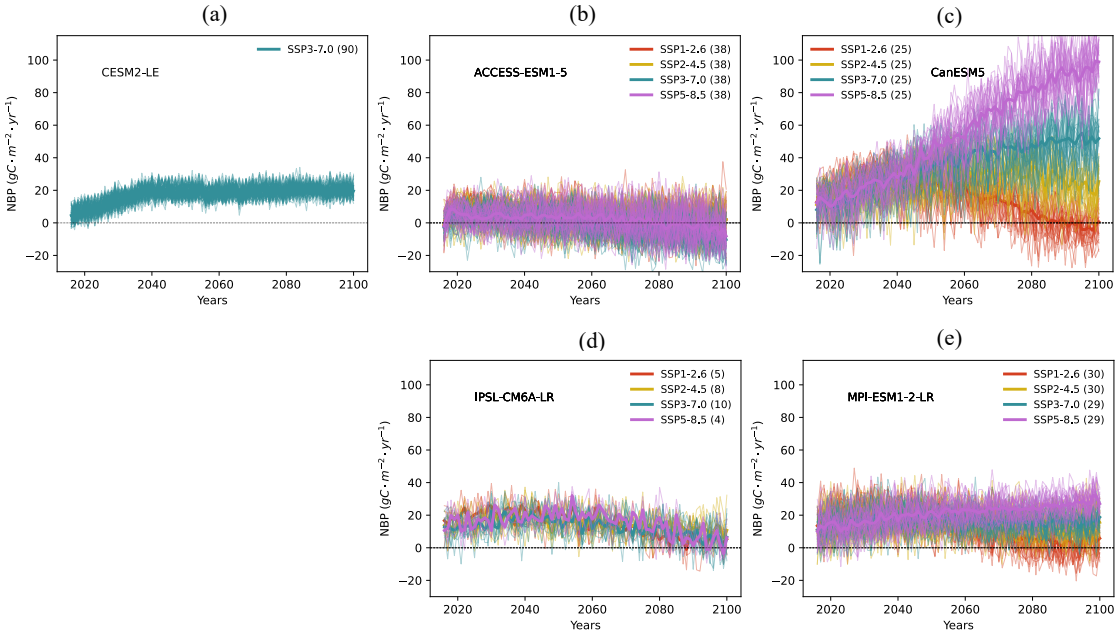

Figure 4. The time series of future NBP from 2016 to 2100 across five ESM large ensembles. The four future scenarios include SSP1-2.6 (red line), SSP2-4.5 (yellow line), SSP3-7.0 (green line), and SSP5-8.5 (purple line). Thin lines represent individual simulations, while thick lines represent the ensemble mean for each scenario. The number of simulations for each model scenario is indicated in the legend next to the scenario label.

3.3 ToE in future projections

We examine the time series of NBP under various future scenarios from 2016 to 2100 (Fig. 4). While NBP trends are similar in the two low CO_2 emission scenarios (SSP1-2.6 and SSP2-4.5), the highest emission scenario (SSP5-8.5) shows large deviations across models.

In CESM2-LE, the SSP3-7.0 scenario shows a steady increase in NBP until around 2040, followed by stable values until 2100. ACCESS-ESM1-5 and IPSL-CM6A-LR exhibit mixed NBP trends in all scenarios, with a relatively stable trend before 2050 and a gradual decline afterwards—ACCESS-ESM1-5 even shifted to a net carbon source. In CanESM5, all scenarios are mixed and together increasing until 2050. After that, all scenarios diverged according to different emission scenarios. MPI-ESM1-2-LR also have all scenarios mixed before around 2050, then diverge clearly with a lower overall trend. Except CanESM5, the large year–to–year variability in NBP makes it challenging to distinguish long-term trends across scenarios.

We then examine the time series of GPP and TER under future scenarios (Appendix A Fig. A.7 and A.8). GPP continues to rise in all models until 2100, except for SSP1-2.6, in which GPP slightly decreases after ca. 2060 (Appendix A Fig. A.7). TER follows a similar pattern, with an increasing trend in line with the different CO_2 emission scenarios (Appendix A Fig. A.8).

https://doi.org/10.5194/egusphere-2025-1924
Preprint. Discussion started: 19 May 2025
© Author(s) 2025. CC BY 4.0 License.

The increase in GPP is likely due to the enhanced CO_2 fertilization and warming in mid-to-high latitudes (Ruehr et al., 2023; O'Sullivan et al., 2022).

Distinguishing the ToE for NBP from different future scenarios is challenging, due to smaller anthropogenic signal and larger year–to–year variations across four future scenarios (Appendix A Fig. A.9). Only CanESM5 shows a clear separation between scenarios, with ToE of 144 years for SSP1-2.6, 57 years for SSP2-4.5, 33 years for SSP3-7.0, and 17 years for SSP5-8.5. Other models take over 44 years to detect the anthropogenic signal among all scenarios. In contrast, GPP and TER trends are more distinct and separated according to different scenarios, resulting in much shorter ToE (Appendix A Fig. A.10, A.11). This might be due to an increase in the CO_2 emission level, or a stronger anthropogenic signal that outweighs the increased noise level, making the detection time more driven by impacts from anthropogenic perturbations rather than internal climate variability.

In future scenarios, it takes longer to detect the anthropogenic signal in NBP, when compared to historical simulations. This delay is likely due to the small anthropogenic signal caused by the compensation effect of GPP and TER, and larger noise levels that driven by more frequent extreme events in a warming climate (Arias et al., 2021), which amplifies year–to–year variations in the land carbon sink. Reducing these year–to–year variations is crucial for reducing the ToE in NBP. In the next section, we apply dynamical adjustment to filter out the atmospheric circulationinduced variability in NBP, and assess whether it can contribute to reduce ToE in both historical simulations and future scenarios.

3.4 Dynamical adjustment for noise reduction

We use the ridge regression to filter out atmospheric circulation induced variability in year–to–year NBP variability (Fig. 5). By applying the ridge regression model that based on sea level pressure as covariates, the circulation induced variability in the respective carbon flux is predicted. The predicted circulation induced variability is assumed to contain direct influences (via thermodynamics or CO_2 fertilization) of climate change (Sippel et al., 2019). Because circulation induced variability is highly variable and often assumed to be largely internal variability, the residual can be expected to show a higher signal-to-noise ratio (e.g., Deser et al. (2016); Sippel et al. (2019)).

The noise of NBP is substantially reduced after filtering out circulation induced variability, so that ToE is reduced in both historical simulations and future scenarios (Fig. 5, Appendix A Table. A.1). In the historical simulations, the relative reduction in ToE ranges from 34.0% (CESM2-LE) to 38.6% (CanESM5). For future scenarios, the reduction ranges from 27.1% to 54.3%, except for ACCESS-ESM1-5, where reductions are mostly less pronounced (Appendix A Table A.1). For GPP, the relative reduction in ToE is smaller (Appendix A Fig. A.12 and Table. A.3). In the historical simulations, it ranges from 12.7% (CanESM5) to 32.1% (ACCESS-ESM1-5), and for future scenarios, the relative reduction ranges from 19.2% to 59.1%. The large reduction of ToE indicates that NBP and GPP are both substantially affected by circulation induced variability.

https://doi.org/10.5194/egusphere-2025-1924
Preprint. Discussion started: 19 May 2025
© Author(s) 2025. CC BY 4.0 License.

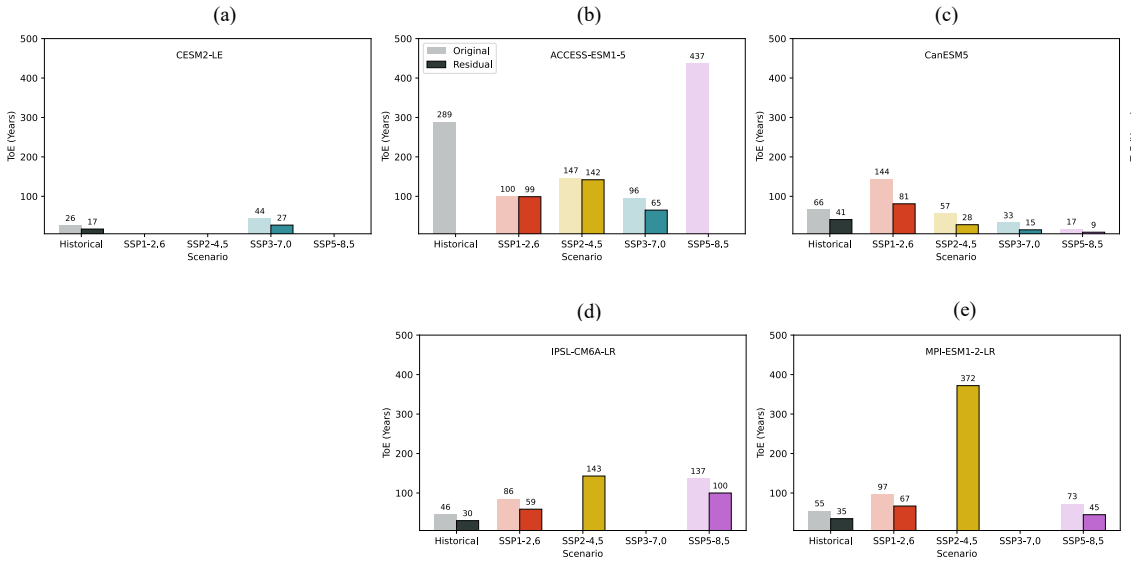

Figure 5. ToE of NBP from historical simulations to future scenarios. Note that ToE in historical simulations is calculated with signal period of 1960–2009 relative to the noise period of 1930–1959, and ToE in future scenarios is calculated with signal period of 2020–2070 relative to the noise period of 2020–2050, details please check Sect. 2.4. The light colored boxes represent the ToE of NBP, while the neighboring darker shaded, black framed boxes represent the ToE of the NBP residual with the circulation induced variability removed. In cases where both boxes are missing, the respective simulation was not available.

4 Conclusions

This study examines the detection of long-term trends driven by anthropogenic signals in the global land carbon sink. Using five ESM large ensembles, we analyze both the historical period (1851–2014) and future scenarios (2016–2100), and find that:

In the historical period, the global land carbon sink (NBP) shows large year–to–year variations, which can enhance or obscure long-term anthropogenic trends. While both carbon uptake (GPP) and ecosystem respiration (TER) show apparent trends influenced by anthropogenic perturbations, their year–to–year variations are relatively small. Since NBP corresponds to the balance between carbon absorption (photosynthesis) and release (ecosystem respiration), as well as other fluxes such as fires, the long-term trend of NBP is in most cases smaller due to this compensation, leaving NBP with a smaller long-term trend and relatively larger year–to–year variations.

We find that the ToE is smaller at global scale compared to regional scales, that is, the anthropogenic signal can be detected earlier at global scale. In the period of 1960-2009, it takes over 26 years for NBP signals to emerge from internal variability, and around 10 years for GPP and TER. At the regional scale, ToE is longer, which might due to larger noise from natural climate variability in most regions. Coarser resolutions reduce the detection time, but the spatial delay is not universal—some high-latitude regions, for example Russia, is found in three CMIP6 models having a shorter detection time of NBP. This is due partly to a smaller noise compared with other regions and the global scale, and partly due to a high signal relative to the small

https://doi.org/10.5194/egusphere-2025-1924
Preprint. Discussion started: 19 May 2025
© Author(s) 2025. CC BY 4.0 License.

average carbon flux at present in those northern regions. The smaller noise may be also due to the small average carbon flux, and associated small variability.

In future scenarios, it takes longer to detect anthropogenic signal in NBP, due to lower anthropogenic signal level caused by the compensation effect of GPP and TER, as well as higher noise levels from more frequent extreme events under a warming climate (Arias et al., 2021). The future trends of global land carbon sink differs significantly across models. While some models have time series separated by emissions after 2050, others remain mixed through 2100. This might be due to the large uncertainty in projections of the global land carbon sink (Friedlingstein et al., 2014; Padrón et al., 2022). For high CO_2 emission scenarios of SSP3-7.0 and SSP5-8.5, CanESM5 continued increasing after around 2050, while other models show a carbon saturation, which might be due to model uncertainties in climate change and nutrient limitations (Arora et al., 2020). Uncertainty in ToE in future projections is closely linked to uncertainties across the model projections of the land carbon sink in the future. In contrast, GPP and TER increase consistently and are well separated by different CO_2 emission scenarios.

NBP exhibits larger year–to–year variability and it is difficult to detect the anthropogenic signal. After removing atmospheric circulation induced variability from NBP, the time of emergence of the anthropogenic signal is significantly reduced. In the historical simulations, the relative reduction in the ToE ranges from 34.0 to 38.6%, while in future scenarios it ranges between 27.1 to 54.3%. Future NBP is more influenced by anthropogenic perturbations and natural variations, with increasing extreme events contributing to the noise (Arias et al., 2021). However, anthropogenic perturbations remain the dominant factor of GPP trends, which determine the time of emergence under all future scenarios. This approach can be applied in observations to facilitate an early detection of anthropogenic signal in global carbon cycle variability.

This study highlights how early the anthropogenic impacts on the global land carbon sink can be detected. By using ridge regression to remove atmospheric circulation induced variability, the detection time can be largely reduced. However, there are still substantial uncertainties across models, with differing patterns and large year–to–year variations (Friedlingstein et al., 2014; Arora et al., 2020). Our proposed approach to use dynamical adjustment to reduce ToE can contribute to enhance our ability to monitor human impacts on land carbon variability and thus support decision making. This approach is particularly helpful in detecting if recent regional carbon flux trend is internal climate variability or forced by climate change. Internally driven trend might not going to be sustained in near-future, while trends forced by climate change can be expected to be the continuation of present trends.

Code availability. The python scripts used for this study is available at Li (2025): Code for PhD thesis: Towards constraining the role of internal climate variability and the forced response in the global carbon cycle, Chapter 4, DOI: 10.5281/zenodo.15264967, version v2, 2025

Data availability. Please check Sect. 2.1 for details.

https://doi.org/10.5194/egusphere-2025-1924
Preprint. Discussion started: 19 May 2025
© Author(s) 2025. CC BY 4.0 License.

Author contributions. Conceptualization by NLi, AB, SS; methodology by NLi, AB, SS, NLin, MR, MM; investigation by NLi, AB, SS, NLin; visualization by NLi; supervision by AB, SS, Nlin, MM, MR; writing original draft by NLi; review by AB, SS, NLin, MM.

Competing interests. The contact author has declared that none of the authors has any competing interests.

Acknowledgements. AI tools ChatGPT (version GPT-4o mini) and Grammarly are used in this manuscript. They helped with writing, including grammar correction and refining sentences and paragraphs. However, the original scientific ideas are from authors.

https://doi.org/10.5194/egusphere-2025-1924
Preprint. Discussion started: 19 May 2025
© Author(s) 2025. CC BY 4.0 License.

Appendix A

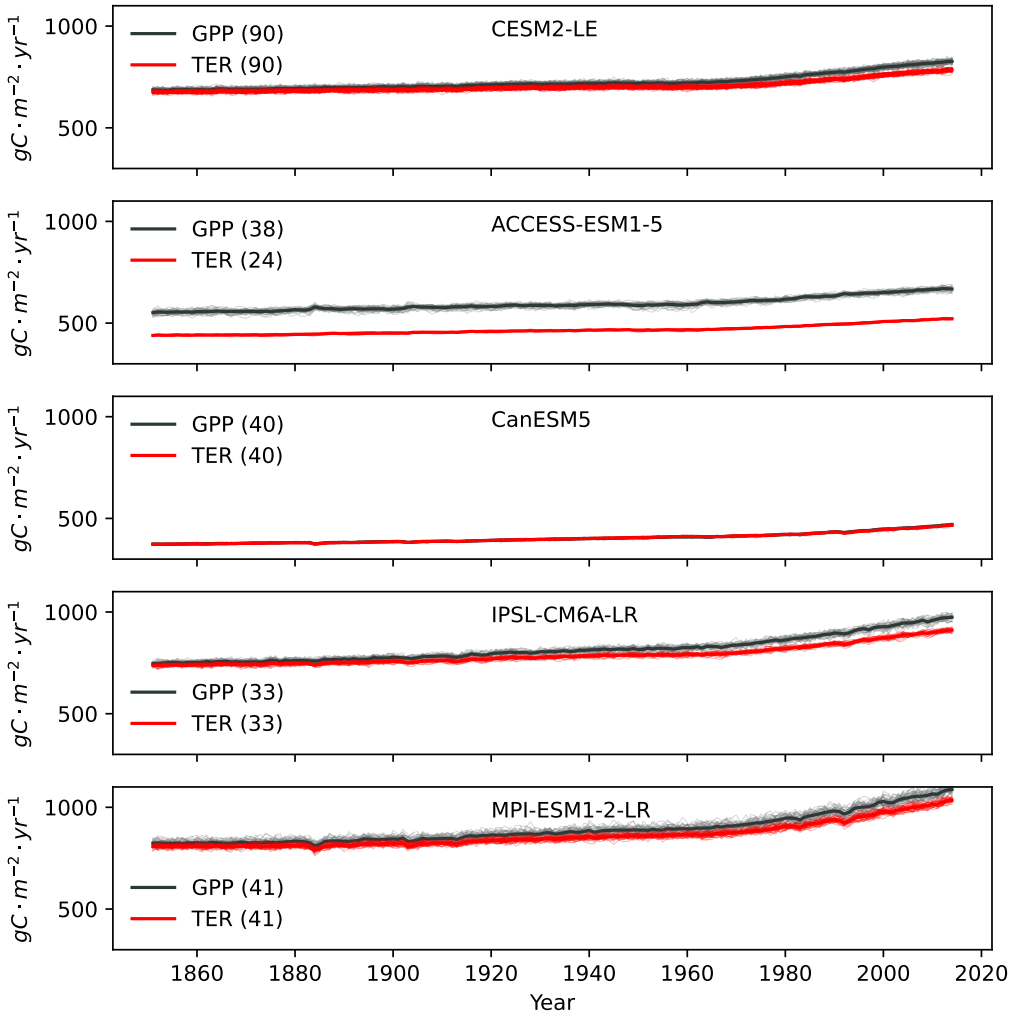

Figure A.1. Time series of GPP (black lines) and TER (red lines) from 1851 to 2014 in five Earth system model large ensembles. Thin lines represent individual simulations, while the bold lines represent the ensemble mean. The number of simulations for each model is listed in the legend next to the model name. In order to have consistent sign with GPP, TER here is multiplied by –1.

https://doi.org/10.5194/egusphere-2025-1924
Preprint. Discussion started: 19 May 2025
© Author(s) 2025. CC BY 4.0 License.

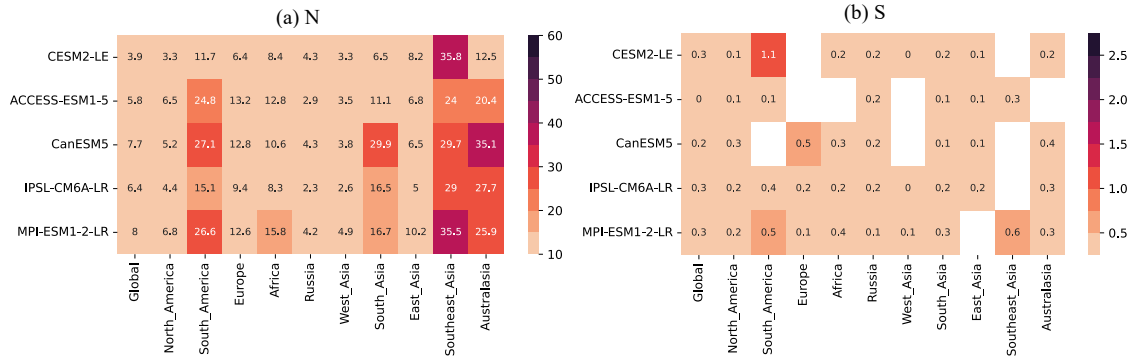

Figure A.2. Heat map of noise and signal of NBP in historical simulations across five Earth system model large ensembles.

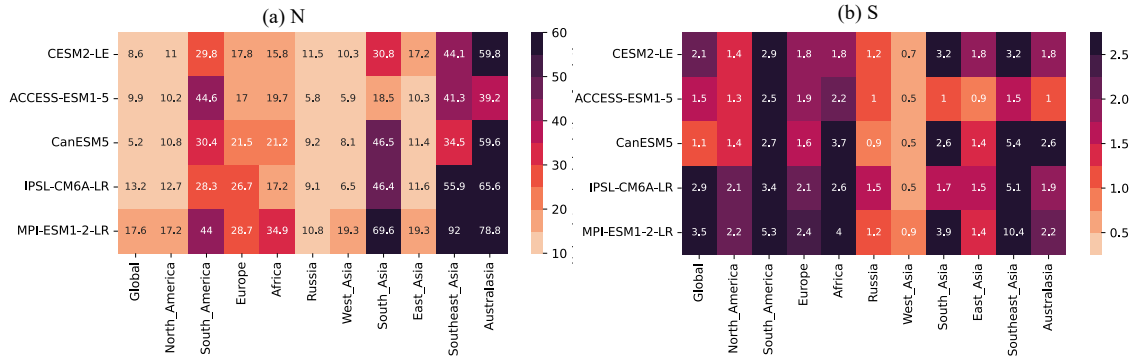

Figure A.3. Heat map of noise and signal of GPP in historical simulations across five Earth system model large ensembles.

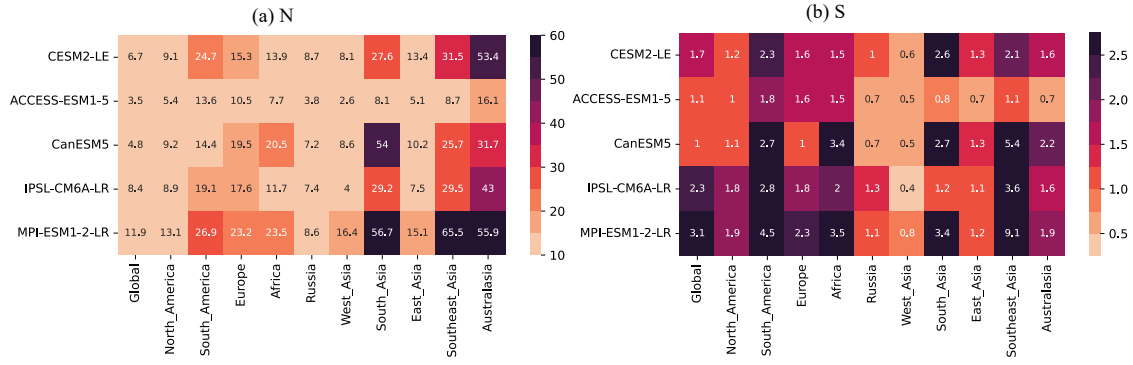

Figure A.4. Heat map of noise and signal in TER in historical simulations across five Earth system model large ensembles.

https://doi.org/10.5194/egusphere-2025-1924
Preprint. Discussion started: 19 May 2025
© Author(s) 2025. CC BY 4.0 License.

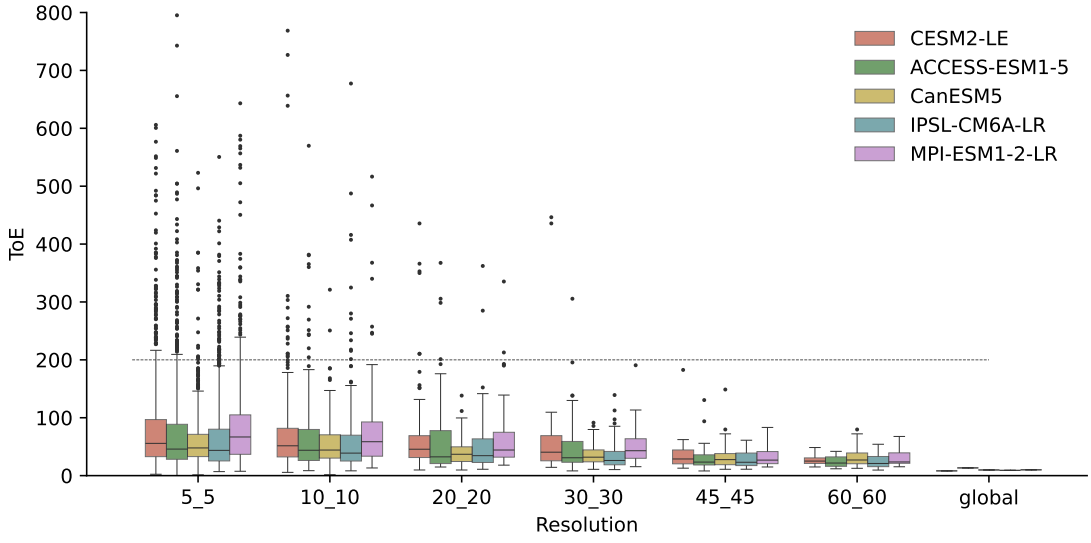

Figure A.5. Spatial effect in GPP historical simulations (1851–2014) across five Earth system model large ensembles. The distribution of time of emergence are shown for varying resolutions.

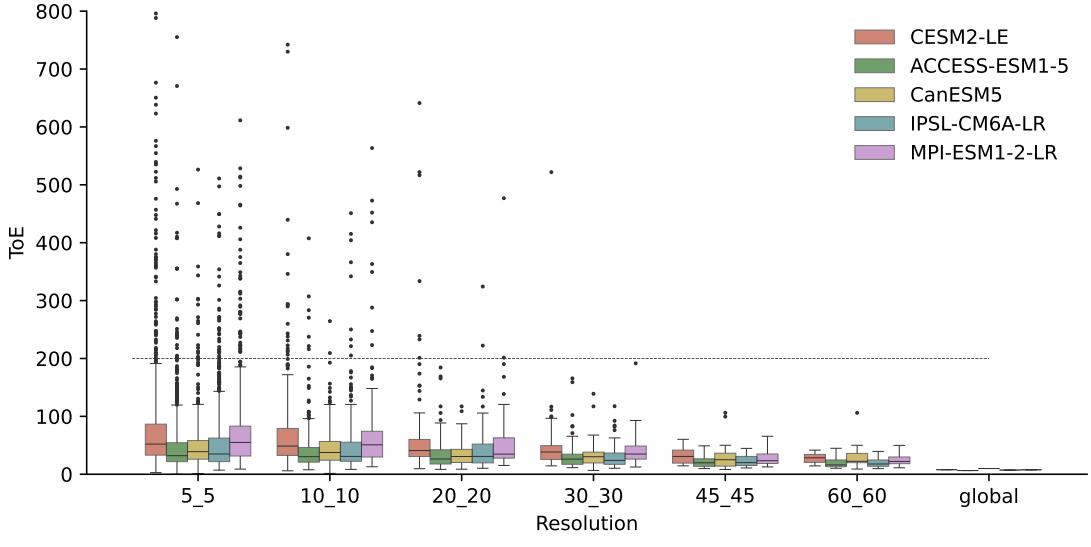

Figure A.6. Spatial effect in TER historical simulations (1851–2014) across five Earth system model large ensembles. The distribution of time of emergence are shown for varying resolutions.

https://doi.org/10.5194/egusphere-2025-1924
Preprint. Discussion started: 19 May 2025
© Author(s) 2025. CC BY 4.0 License.

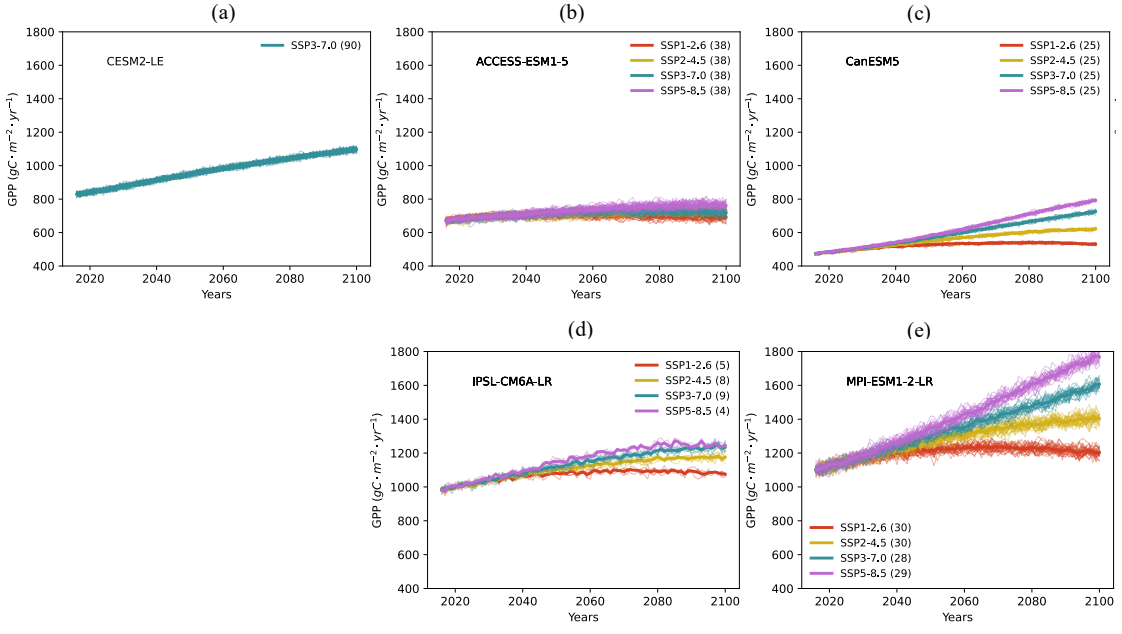

Figure A.7. The time series of future GPP from 2016 to 2100 across five Earth system model large ensembles. The four future scenarios include SSP1-2.6 (red line), SSP2-4.5 (yellow line), SSP3-7.0 (green line), and SSP5-8.5 (purple line). Thin lines represent individual simulations, while thick lines represent the ensemble mean for each scenario. The number of simulations for each model scenario is indicated in the legend next to the scenario label.

https://doi.org/10.5194/egusphere-2025-1924
Preprint. Discussion started: 19 May 2025
© Author(s) 2025. CC BY 4.0 License.

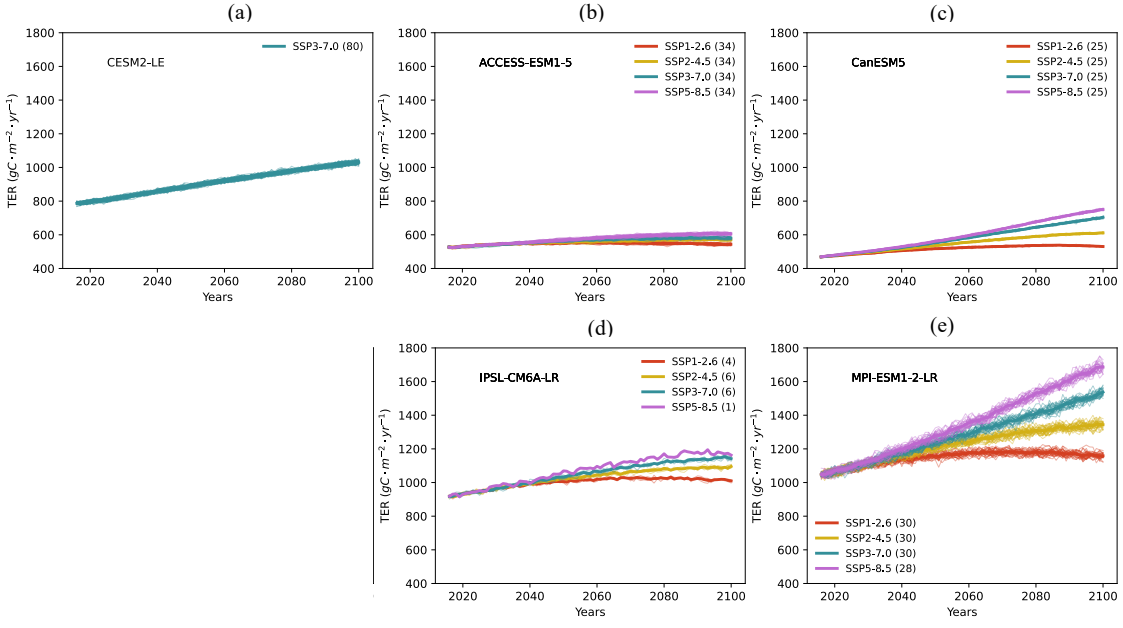

Figure A.8. The time series of future TER from 2016 to 2100 across five Earth system model large ensembles. The four future scenarios include SSP1-2.6 (red line), SSP2-4.5 (yellow line), SSP3-7.0 (green line), and SSP5-8.5 (purple line). Thin lines represent individual simulations, while thick lines represent the ensemble mean for each scenario. The number of simulations for each model scenario is indicated in the legend next to the scenario label.

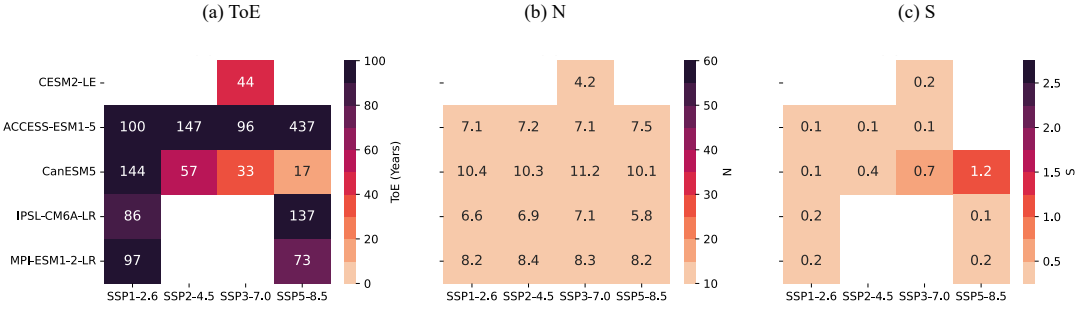

Figure A.9. Heat map of ToE, noise, and signal of NBP under future scenarios.

https://doi.org/10.5194/egusphere-2025-1924
Preprint. Discussion started: 19 May 2025
© Author(s) 2025. CC BY 4.0 License.

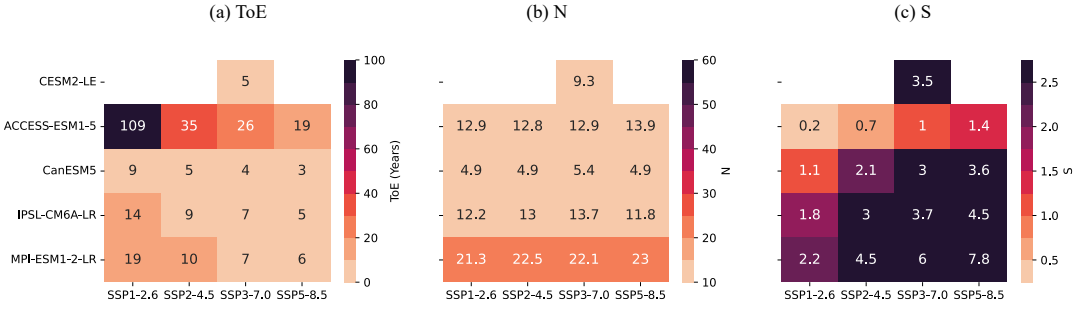

Figure A.10. Heat map of ToE, noise, and signal of GPP under future scenarios.

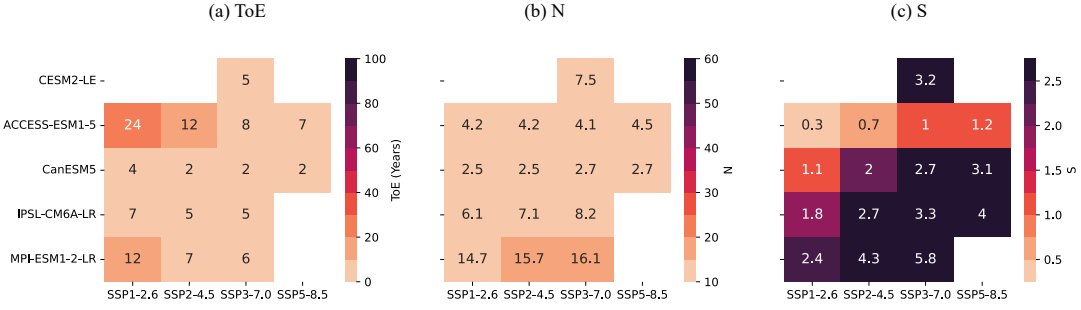

Figure A.11. Heat map of ToE, noise, and signal of TER under future scenarios.

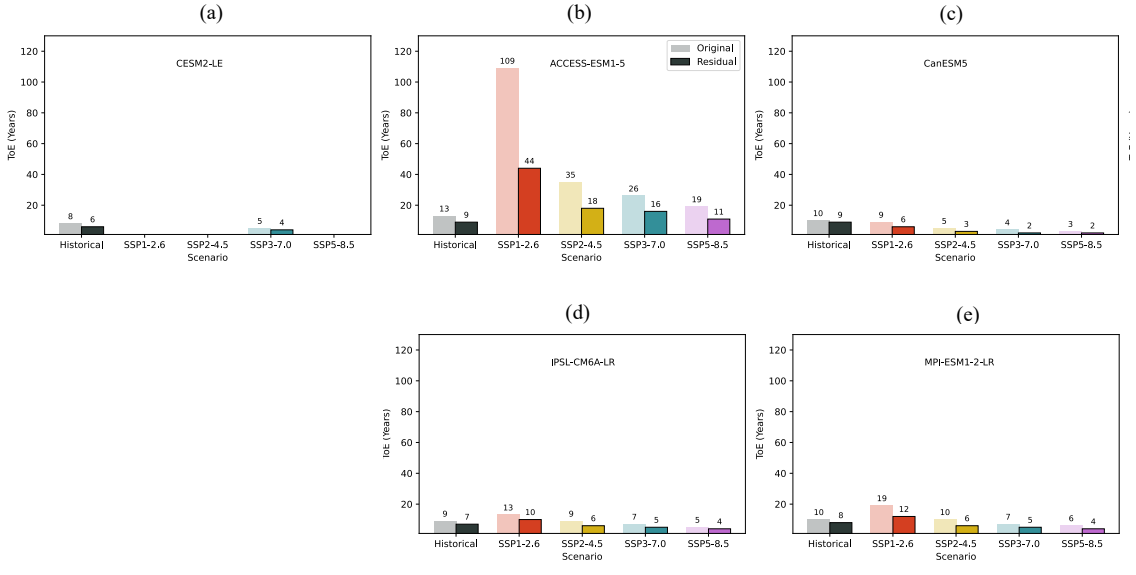

Figure A.12. ToE of GPP from historical simulations to future scenarios. The light colored boxes represent the ToE of GPP, while the neighboring darker shade, black framed boxes represent the ToE of the GPP residual, which has the circulation induced variability removed.

https://doi.org/10.5194/egusphere-2025-1924
Preprint. Discussion started: 19 May 2025
© Author(s) 2025. CC BY 4.0 License.

Relative change (%)	CESM2-LE	ACCESS-ESM1-5	CanESM5	IPSL-CM6A-LR	MPI-ESM1-2-LR
Historical	34.0	-	38.6	35.0	35.5
SSP1-2.6	-	1.0	43.7	32.1	30.6
SSP2-4.5	-	3.3	50.4	-	-
SSP3-7.0	38.1	32.2	54.3	-	-
SSP5-8.5	-	-	48.2	27.1	38.8

Table A.1. ToE reduction in NBP, calculated according to Eq. (4).

Relative change (%)	CESM2-LE	ACCESS-ESM1-5	CanESM5	IPSL-CM6A-LR	MPI-ESM1-2-LR
Historical	35.5	34.1	48.3	39.2	39.1
SSP1-2.6	-	35.8	53.8	25.9	34.9
SSP2-4.5	-	39.1	52.2	32.8	40.0
SSP3-7.0	36.9	37.0	54.7	34.7	36.7
SSP5-8.5	-	39.0	48.6	18.3	38.0

Table A.2. Noise reduction in NBP, calculated according to Eq. (4).

Relative change (%)	CESM2-LE	ACCESS-ESM1-5	CanESM5	IPSL-CM6A-LR	MPI-ESM1-2-LR
Historical	24.8	32.1	12.7	26.4	24.8
SSP1-2.6	-	59.1	34.3	25.6	36.5
SSP2-4.5	-	47.5	32.4	27.8	39.5
SSP3-7.0	22.6	39.2	39.9	30.3	35.8
SSP5-8.5	-	42.9	29.6	19.2	37.6

Table A.3. ToE reduction in GPP, calculated according to Eq. (4).

https://doi.org/10.5194/egusphere-2025-1924
Preprint. Discussion started: 19 May 2025
© Author(s) 2025. CC BY 4.0 License.

Relative change (%)	CESM2-LE	ACCESS-ESM1-5	CanESM5	IPSL-CM6A-LR	MPI-ESM1-2-LR
Historical	25.8	32.5	14.4	28.0	26.7
SSP1-2.6	-	38.0	34.1	26.1	36.1
SSP2-4.5	-	41.3	32.7	27.9	39.1
SSP3-7.0	22.4	38.6	40.0	30.5	36.2
SSP5-8.5	-	41.5	29.7	18.8	37.9

Table A.4. Noise reduction in GPP, calculated according to Eq. (4).

https://doi.org/10.5194/egusphere-2025-1924
Preprint. Discussion started: 19 May 2025
© Author(s) 2025. CC BY 4.0 License.

References

Arias, P. A., Bellouin, N., Coppola, E., Jones, R. G., Krinner, G., Marotzke, J., Naik, B., Palmer, M. D., Plattner, G. K., Rogelj, J., Rojas, M., Sillmann, J., Storelvmo, T., Thorne, P. W., Trewin, B., Achuta Rao, K., Adhikary, B., Allan, R. P., Armour, K., Bala, G., Barimalala, R., Berger, S., Canadell, J. G., Cassou, C., Cherchi, A., Collins, W., Collins, W. D., Connors, S. L., Corti, S., Cruz, F., Dentener, F. J., Dereczynski, C., Di Luca, A., Diongue Niang, A., Doblas-Reyes, F. J., Dosio, A., Douville, H., Engelbrecht, F., Eyring, V., Fischer, E., Forster, P., Fox-Kemper, B., Fuglestvedt, J. S., Fyfe, J. C., Gillett, N. P., Goldfarb, L., Gorodetskaya, I., Gutierrez, J. M., Hamdi, R., Hawkins, E., Hewitt, H. T., Hope, P., Islam, A. S., Jones, C., Kaufman, D. S., Kopp, R. E., Kosaka, Y., Kossin, J., Krakovska, S., Lee, J. Y., Li, J., Mauritsen, T., Maycock, T. K., Meinshausen, M., Min, S. K., Monteiro, P. M. S., Ngo-Duc, T., Otto, F., Pinto, I., Pirani, A., Raghavan, K., Ranasinghe, R., Ruane, A. C., Ruiz, L., Sallée, J. B., Samset, B. H., Sathyendranath, S., Seneviratne, S. I., Sörensson, A. A., Szopa, S., Takayabu, I., Tréguier, A. M., van den Hurk, B., Vautard, R., von Schuckmann, K., Zaehle, S., Zhang, X., and Zickfeld, K.: Technical Summary. In Climate Change 2021: The Physical Science Basis. Contribution of Working Group I to the Sixth Assessment Report of the Intergovernmental Panel on Climate Change, Cambridge University Press, Cambridge, United Kingdom and New York, NY, USA, doi:10.1017/9781009157896.002, p33-144, 114-115, 2021.

Arora, V. K., Katavouta, A., Williams, R. G., Jones, C. D., Brovkin, V., Friedlingstein, P., Schwinger, J., Bopp, L., Boucher, O., Cadule, P., Chamberlain, M. A., Christian, J. R., Delire, C., Fisher, R. A., Hajima, T., Ilyina, T., Joetzjer, E., Kawamiya, M., Koven, C. D., Krasting, J. P., Law, R. M., Lawrence, D. M., Lenton, A., Lindsay, K., Pongratz, J., Raddatz, T., Séférian, R., Tachiiri, K., Tjiputra, J. F., Wiltshire, A., Wu, T., and Ziehn, T.: Carbon–concentration and carbon–climate feedbacks in CMIP6 models and their comparison to CMIP5 models, Biogeosciences, 17, 4173–4222, https://doi.org/10.5194/bg-17-4173-2020, 2020.

Bacastow, R. B.: Modulation of atmospheric carbon dioxide by the Southern Oscillation, Nature, 261, 116–118, https://doi.org/10.1038/261116a0, 1976.

Bonan, G., Lombardozzi, D. L., and Wieder, W. R.: The signature of internal variability in the terrestrial carbon cycle, Environ. Res. Lett., 16, 034 022, https://doi.org/10.1088/1748-9326/abd6a9, 2021.

Boucher, O., Servonnat, J., Albright, A. L., Aumont, O., Balkanski, Y., Bastrikov, V., Bekki, S., Bonnet, R., Bony, S., Bopp, L., Braconnot, P., Brockmann, P., Cadule, P., Caubel, A., Cheruy, F., Codron, F., Cozic, A., Cugnet, D., D'Andrea, F., Davini, P., de Lavergne, C., Denvil, S., Deshayes, J., Devilliers, M., Ducharne, A., Dufresne, J.-L., Dupont, E., Éthé, C., Fairhead, L., Falletti, L., Flavoni, S., Foujols, M.-A., Gardoll, S., Gastineau, G., Ghattas, J., Grandpeix, J.-Y., Guenet, B., Guez, Lionel, E., Guilyardi, E., Guimberteau, M., Hauglustaine, D., Hourdin, F., Idelkadi, A., Joussaume, S., Kageyama, M., Khodri, M., Krinner, G., Lebas, N., Levavasseur, G., Lévy, C., Li, L., Lott, F., Lurton, T., Luyssaert, S., Madec, G., Madeleine, J.-B., Maignan, F., Marchand, M., Marti, O., Mellul, L., Meurdesoif, Y., Mignot, J., Musat, I., Ottlé, C., Peylin, P., Planton, Y., Polcher, J., Rio, C., Rochetin, N., Rousset, C., Sepulchre, P., Sima, A., Swingedouw, D., Thiéblemont, R., Traore, A. K., Vancoppenolle, M., Vial, J., Vialard, J., Viovy, N., and Vuichard, N.: Presentation and evaluation of the IPSL-CM6A-LR Climate Model, Journal of Advances in Modeling Earth Systems, 12, e2019MS002 010, https://doi.org/10.1029/2019MS002010, 2020.

Brunner, L., Hauser, M., Lorenz, R., and Beyerle, U.: The ETH Zurich CMIP6 next generation archive: technical documentation., Zenodo, https://doi.org/10.5281/zenodo.3734128, 2020.

Canadell, J. G., Monteiro, P. M. S., Costa, M. H., Cotrim da Cunha, L., Cox, P. M., Eliseev, A. V., Henson, S., Ishii, M., Jaccard, S., Koven, C., Lohila, A., Patra, P. K., Piao, S., Rogelj, J., Syampungani, S., Zaehle, S., and Zickfeld, K.: Global Carbon and other Biogeochemical Cycles and Feedbacks. In Climate Change 2021: The Physical Science Basis. Contribution of Working Group I to the Sixth Assessment

https://doi.org/10.5194/egusphere-2025-1924
Preprint. Discussion started: 19 May 2025
© Author(s) 2025. CC BY 4.0 License.

Report of the Intergovernmental Panel on Climate Change, Cambridge University Press, Cambridge, United Kingdom and New York, NY, USA, https://doi.org/10.1017/9781009157896.007, chapter 5, p732, 2021.

Chen, D., Rojas, M., Samset, B. H., Cobb, K., Diongue Niang, A., Edwards, P., Emori, S., Faria, S. H., Hawkins, E., Hope, P., Huybrechts, P., Meinshausen, M., Mustafa, S. K., Plattner, G.-K., and Tréguier, A.-M.: Framing, Context, and Methods. In Climate Change 2021: The Physical Science Basis. Contribution of Working Group I to the Sixth Assessment Report of the Intergovernmental Panel on Climate Change, Cambridge University Press, Cambridge, United Kingdom and New York, NY, USA, https://doi.org/10.1017/9781009157896.003, chapter 1, p194, 233, 2021.

Ciais, P., Bastos, A., Chevallier, F., Lauerwald, R., Poulter, B., Canadell, J. G., Hugelius, G., Jackson, R. B., Jain, A., Jones, M., Kondo, M., Luijkx, I. T., Patra, P. K., Peters, W., Pongratz, J., Petrescu, A. M. R., Piao, S., Qiu, C., Von Randow, C., Regnier, P., Saunois, M., Scholes, R., Shvidenko, A., Tian, H., Yang, H., Wang, X., and Zheng, B.: Definitions and methods to estimate regional land carbon fluxes for the second phase of the regional Carbon Cycle Assessment and Processes Project (RECCAP-2), Geoscientific Model Development, 15, 1289–1316, https://doi.org/10.5194/gmd-15-1289-2022, 2022.

Danabasoglu, G., Lamarque, J.-F., Bacmeister, J., Bailey, D. A., DuVivier, A. K., Edwards, J., Emmons, L. K., Fasullo, J., Garcia, R., Gettelman, A., Hannay, C., Holland, M. M., Large, W. G., Lauritzen, P. H., Lawrence, D. M., Lenaerts, J. T. M., Lindsay, K., Lipscomb, W. H., Mills, M. J., Neale, R., Oleson, K. W., Otto-Bliesner, B., Phillips, A. S., Sacks, W., Tilmes, S., van Kampenhout, L., Vertenstein, M., Bertini, A., Dennis, J., Deser, C., Fischer, C., Fox-Kemper, B., Kay, J. E., Kinnison, D., Kushner, P. J., Larson, V. E., Long, M. C., Mickelson, S., Moore, J. K., Nienhouse, E., Polvani, L., Rasch, P. J., and Strand, W. G.: The Community Earth System Model Version 2 (CESM2), Journal of Advances in Modeling Earth Systems, 12, e2019MS001 916, https://doi.org/10.1029/2019MS001916, 2020.

Deser, C., Phillips, A., Bourdette, V., and Teng, H.: Uncertainty in climate change projections: the role of internal variability, Climate Dynamics, 38, 527–546, https://doi.org/10.1007/s00382-010-0977-x, 2012a.

Deser, C., Knutti, R., Solomon, S., et al.: Communication of the role of natural variability in future North American climate, Nat. Clim. Change, 2, 775–779, https://doi.org/10.1038/nclimate1562, 2012b.

Deser, C., Terray, L., and Phillips, A. S.: Forced and Internal Components of Winter Air Temperature Trends over North America during the past 50 Years: Mechanisms and Implications, Journal of Climate, 29(6), 2237–2258, https://doi.org/10.1175/JCLI-D-15-0304.1, 2016.

Deser, C., Lehner, F., Rodgers, K. B., Ault, T., Delworth, T. L., DiNezio, P. N., Fiore, A., Frankignoul, C., Fyfe, J. C., Horton, D. E., Kay, J. E., Knutti, R., Lovenduski, N. S., Marotzke, J., McKinnon, K. A., Minobe, S., Randerson, J., Screen, J. A., Simpson, I. R., and Ting, M.: Insights from Earth system model initial-condition large ensembles and future prospects, Nature Climate Change, 10, 277–286, https://doi.org/10.1038/s41558-020-0731-2, 2020.

Doblas-Reyes, F. J., Sörensson, A. A., Almazroui, M., Dosio, A., Gutowski, W. J., Haarsma, R., Hamdi, R., Hewitson, B., Kwon, W. T., Lamptey, B. l., Maraun, D., Stephenson, T. S., Takayabu, I., Terray, L., Turner, A., and Zuo, Z.: Linking Global to Regional Climate Change. In Climate Change 2021: The Physical Science Basis. Contribution of Working Group I to the Sixth Assessment Report of the Intergovernmental Panel on Climate Change, Cambridge University Press, Cambridge, United Kingdom and New York, NY, USA, https://doi.org/10.1017/9781009157896.012, iPCC,2021, chapter 10, p1363-1512, 2021.

Eyring, V., Bony, S., Meehl, G. A., Senior, C. A., Stevens, B., Stouffer, R. J., and Taylor, K. E.: Overview of the Coupled Model Intercomparison Project Phase 6 (CMIP6) experimental design and organization, Geoscientific Model Development, 9, 1937–1958, https://doi.org/10.5194/gmd-9-1937-2016, 2016.

Eyring, V., Gillett, N. P., Achuta Rao, K. M., Barimalala, R., Barreiro Parrillo, M., Bellouin, N., Cassou, C., Durack, P. J., Kosaka, Y., McGregor, S., Min, S., Morgenstern, O., and Sun, Y.: Human Influence on the Climate System. In Climate Change 2021: The Physical

https://doi.org/10.5194/egusphere-2025-1924
Preprint. Discussion started: 19 May 2025
© Author(s) 2025. CC BY 4.0 License.

Science Basis. Contribution of Working Group I to the Sixth Assessment Report of the Intergovernmental Panel on Climate Change, Cambridge University Press, Cambridge, United Kingdom and New York, NY, USA, https://doi.org/10.1017/9781009157896.005, chapter 3, p425, 446, 2021.

Frankcombe, L. M., England, M. H., Mann, M. E., and Steinman, B. A.: Separating Internal Variability from the Externally Forced Climate Response, Journal of Climate, 28, 8184 – 8202, https://doi.org/10.1175/JCLI-D-15-0069.1, 2015.

Friedlingstein, P., Meinshausen, M., Arora, V. K., Jones, C. D., Anav, A., Liddicoat, S. K., and Knutti, R.: Uncertainties in CMIP5 climate projections due to carbon cycle feedbacks, Journal of Climate, 27(2), 511–526, https://doi.org/10.1175/JCLI-D-12-00579.1, 2014.

Friedlingstein, P., Jones, M. W., O'Sullivan, M., Andrew, R. M., Bakker, D. C. E., Hauck, J., Le Quéré, C., Peters, G. P., Peters, W., Pongratz, J., Sitch, S., Canadell, J. G., Ciais, P., Jackson, R. B., Alin, S. R., Anthoni, P., Bates, N. R., Becker, M., Bellouin, N., Bopp, L., Chau, T. T. T., Chevallier, F., Chini, L. P., Cronin, M., Currie, K. I., Decharme, B., Djeutchouang, L. M., Dou, X., Evans, W., Feely, R. A., Feng, L., Gasser, T., Gilfillan, D., Gkritzalis, T., Grassi, G., Gregor, L., Gruber, N., Gürses, O., Harris, I., Houghton, R. A., Hurtt, G. C., Iida, Y., Ilyina, T., Luijkx, I. T., Jain, A., Jones, S. D., Kato, E., Kennedy, D., Klein Goldewijk, K., Knauer, J., Korsbakken, J. I., Körtzinger, A., Landschützer, P., Lauvset, S. K., Lefèvre, N., Lienert, S., Liu, J., Marland, G., McGuire, P. C., Melton, J. R., Munro, D. R., Nabel, J. E. M. S., Nakaoka, S.-I., Niwa, Y., Ono, T., Pierrot, D., Poulter, B., Rehder, G., Resplandy, L., Robertson, E., Rödenbeck, C., Rosan, T. M., Schwinger, J., Schwingshackl, C., Séférian, R., Sutton, A. J., Sweeney, C., Tanhua, T., Tans, P. P., Tian, H., Tilbrook, B., Tubiello, F., van der Werf, G. R., Vuichard, N., Wada, C., Wanninkhof, R., Watson, A. J., Willis, D., Wiltshire, A. J., Yuan, W., Yue, C., Yue, X., Zaehle, S., and Zeng, J.: Global Carbon Budget 2021, Earth System Science Data, 14, 1917–2005, https://doi.org/10.5194/essd-14-1917-2022, 2022.

Hastie, T., Tibshirani, R., and Friedman, J.: The elements of statistical learning: data mining, inferencee, and prediction, Springer Series in Statistics, https://doi.org/10.1007/b94608, p61-67, 2009.

Hawkins, E. and Sutton, R.: Time of emergence of climate signals, Geophysical Research Letters, 39, https://doi.org/10.1029/2011GL050087, 2012.

IPCC: Climate Change 2021: The Physical Science Basis. Contribution of Working Group I to the Sixth Assessment Report of the Intergovernmental Panel on Climate Change [Masson-Delmotte, V., P. Zhai, A. Pirani, S.L. Connors, C. Péan, S. Berger, N. Caud, Y. Chen, L. Goldfarb, M.I. Gomis, M. Huang, K. Leitzell, E. Lonnoy, J.B.R. Matthews, T.K. Maycock, T. Waterfield, O. Yelekçi, R. Yu, and B. Zhou (eds.)], 2391, Cambridge University Press, Cambridge, United Kingdom and New York, NY, USA, https://doi.org/10.1017/9781009157896, p115, 2021.

Jung, M., Reichstein, M., Schwalm, C. R., Huntingford, C., Sitch, S., Ahlström, A., Arneth, A., Camps-Valls, G., Ciais, P., Friedlingstein, P., Gans, F., Ichii, K., Jain, A. K., Kato, E., Papale, D., Poulter, B., Raduly, B., Rödenbeck, C., Tramontana, G., Viovy, N., Wang, Y.-P., Weber, U., Zaehle, S., and Zeng, N.: Compensatory water effects link yearly global land CO_2 sink changes to temperature, Nature, 541, 516–520, https://doi.org/10.1038/nature20780, 2017.

Kay, J. E., Deser, C., Phillips, A., Mai, A., Hannay, C., Strand, G., Arblaster, J. M., Bates, S. C., Danabasoglu, G., Edwards, J., Holland, M., Kushner, P., Lamarque, J.-F., Lawrence, D., Lindsay, K., Middleton, A., Munoz, E., Neale, R., Oleson, K., Polvani, L., and Vertenstein, M.: The Community Earth System Model (CESM) Large Ensemble Project: A community resource for studying climate change in the presence of internal climate variability, Bulletin of the American Meteorological Society, 96, 1333–1349, https://doi.org/10.1175/BAMS-D-13-00255.1, 2015.

Keeling, C. D., Whorf, T. P., Wahlen, M., and van der Plichtt, J.: Interannual extremes in the rate of rise of atmospheric carbon dioxide since 1980., Nature, 375, 666–670, https://doi.org/10.1038/375666a0, 1995.

https://doi.org/10.5194/egusphere-2025-1924
Preprint. Discussion started: 19 May 2025
© Author(s) 2025. CC BY 4.0 License.

Kumar, S., Kinter III, J. L., Pan, Z., and Sheffield, J.: Twentieth century temperature trends in CMIP3, CMIP5, and CESM-LE climate simulations: Spatial-temporal uncertainties, differences, and their potential sources, Journal of Geophysical Research: Atmospheres, 121, 9561–9575, https://doi.org/10.1002/2015JD024382, 2016.

Lee, J. Y., Marotzke, J., Bala, G., Cao, L., Corti, S., Dunne, J. P., Engelbrecht, F., Fischer, E., Fyfe, J. C., Jones, C., Maycock, A., Mutemi, J., Ndiaye, O., Panickal, S., and Zhou, T.: Future Global Climate: Scenario-Based Projections and Near- Term Information. In Climate Change 2021: The Physical Science Basis. Contribution of Working Group I to the Sixth Assessment Report of the Intergovernmental Panel on Climate Change, Cambridge University Press, Cambridge, United Kingdom and New York, NY, USA, https://doi.org/10.1017/9781009157896.006, pp. 555, IPCC2021, Chapter 4, 2021.

Lehner, F., Deser, C., and Terray, L.: Toward a New Estimate of "Time of Emergence" of Anthropogenic Warming: Insights from Dynamical Adjustment and a Large Initial-Condition Model Ensemble, Journal of Climate, 30, 7739 – 7756, https://doi.org/10.1175/JCLI-D-16-0792.1, 2017.

Li, N.: Towards-constraining-the-role-of-internal-climate-variability-and-the-forced-response-in-the-global-: Code for PhD thesis: Towards constraining the role of internal climate variability and the forced response in the global carbon cycle, Chapter 4, Zenodo, https://doi.org/10.5281/zenodo.15264967, version v2, 2025.

Li, N., Sippel, S., Winkler, A. J., Mahecha, M. D., Reichstein, M., and Bastos, A.: Interannual global carbon cycle variations linked to atmospheric circulation variability, Earth System Dynamics, 13, 1505–1533, https://doi.org/10.5194/esd-13-1505-2022, 2022.

Lombardozzi, D., Bonan, G. B., and Nychka, D. W.: The emerging anthropogenic signal in land–atmosphere carbon-cycle coupling, Nature Climate Change, 4, 796–800, https://doi.org/10.1038/nclimate2323, 2014.

Maher, N., Milinski, S., Suarez-Gutierrez, L., Botzet, M., Dobrynin, M., Kornblueh, L., Kröger, J., Takano, Y., Ghosh, R., Hedemann, C., Li, C., Li, H., Manzini, E., Notz, D., Putrasahan, D., Boysen, L., Claussen, M., Ilyina, T., Olonscheck, D., Raddatz, T., Stevens, B., and Marotzke, J.: The Max Planck Institute Grand Ensemble: Enabling the Exploration of Climate System Variability, Journal of Advances in Modeling Earth Systems, 11, 2050–2069, https://doi.org/https://doi.org/10.1029/2019MS001639, 2019.

Mahlstein, I., Knutti, R., Solomon, S., and Portmann, R. W.: Early onset of significant local warming in low latitude countries, Environmental Research Letters, 6, 034 009, https://doi.org/10.1088/1748-9326/6/3/034009, 2011.

Mahlstein, I., Hegerl, G., and Solomon, S.: Emerging local warming signals in observational data, Geophysical Research Letters, 39, https://doi.org/10.1029/2012GL053952, 2012.

Mauritsen, T., Bader, J., Becker, T., Behrens, J., Bittner, M., Brokopf, R., Brovkin, V., Claussen, M., Crueger, T., Esch, M., Fast, I., Fiedler, S., Fläschner, D., Gayler, V., Giorgetta, M., Goll, D. S., Haak, H., Hagemann, S., Hedemann, C., Hohenegger, C., Ilyina, T., Jahns, T., Jimenéz-de-la Cuesta, D., Jungclaus, J., Kleinen, T., Kloster, S., Kracher, D., Kinne, S., Kleberg, D., Lasslop, G., Kornblueh, L., Marotzke, J., Matei, D., Meraner, K., Mikolajewicz, U., Modali, K., Möbis, B., Müller, W. A., Nabel, J. E. M. S., Nam, C. C. W., Notz, D., Nyawira, S.-S., Paulsen, H., Peters, K., Pincus, R., Pohlmann, H., Pongratz, J., Popp, M., Raddatz, T. J., Rast, S., Redler, R., Reick, C. H., Rohrschneider, T., Schemann, V., Schmidt, H., Schnur, R., Schulzweida, U., Six, K. D., Stein, L., Stemmler, I., Stevens, B., von Storch, J.-S., Tian, F., Voigt, A., Vrese, P., Wieners, K.-H., Wilkenskjeld, S., Winkler, A., and Roeckner, E.: Developments in the MPI-M Earth System Model version 1.2 (MPI-ESM1.2) and its response to increasing CO_2, Journal of Advances in Modeling Earth Systems, 11, 998–1038, https://doi.org/10.1029/2018MS001400, 2019.

Mercado, L. M., Bellouin, N., Sitch, S., Boucher, O., Huntingford, C., Wild, M., and Cox, P. M.: Impact of changes in diffuse radiation on the global land carbon sink, Nature, 458, 1014–1017, https://doi.org/10.1038/nature07949, 2009.

https://doi.org/10.5194/egusphere-2025-1924
Preprint. Discussion started: 19 May 2025
© Author(s) 2025. CC BY 4.0 License.

Milinski, S., Maher, N., and Olonscheck, D.: How large does a large ensemble need to be?, Earth System Dynamics, 11, 885–901, https://doi.org/10.5194/esd-11-885-2020, 2020.

O'Neill, B. C., Tebaldi, C., van Vuuren, D. P., Eyring, V., Friedlingstein, P., Hurtt, G., Knutti, R., Kriegler, E., Lamarque, J.-F., Lowe, J., Meehl, G. A., Moss, R., Riahi, K., and Sanderson, B. M.: The Scenario Model Intercomparison Project (ScenarioMIP) for CMIP6, Geoscientific Model Development, 9, 3461–3482, https://doi.org/10.5194/gmd-9-3461-2016, 2016.

O'Sullivan, M., Friedlingstein, P., Sitch, S., Anthoni, P., Arneth, A., Arora, V. K., Bastrikov, V., Delire, C., Goll, D. S., Jain, A., Kato, E., Kennedy, D., Knauer, J., Lienert, S., Lombardozzi, D., McGuire, P. C., Melton, J. R., Nabel, J. E. M. S., Pongratz, J., Poulter, B., Séférian, R., Tian, H., Vuichard, N., Walker, A. P., Yuan, W., Yue, X., and Zaehle, S.: Process-oriented analysis of dominant sources of uncertainty in the land carbon sink, Nature Communications, 13, 4781, https://doi.org/10.1038/s41467-022-32416-8, 2022.

Padrón, R. S., Gudmundsson, L., Liu, L., Humphrey, V., and Seneviratne, S. I.: Drivers of intermodel uncertainty in land carbon sink projections, Biogeosciences, 19, 5435–5448, https://doi.org/10.5194/bg-19-5435-2022, 2022.

Piao, S., Wang, X., Wang, K., Li, X., Bastos, A., Canadell, J. G., Ciais, P., Friedlingstein, P., and Sitch, S.: Interannual variation of terrestrial carbon cycle: Issues and perspectives, Global Change Biology, 26, 300–318, https://doi.org/10.1111/gcb.14884, 2020.

Ranasinghe, R., Ruane, A. C., Vautard, R., Arnell, N., Coppola, E., Cruz, F. A., Dessai, S., Islam, A. S., Rahimi, M., Ruiz Carrascal, D., Sillmann, J., Sylla, M. B., Tebaldi, C., Wang, W., and Zaaboul, R.: Climate Change Information for Regional Impact and for Risk Assessment. In Climate Change 2021: The Physical Science Basis. Contribution of Working Group I to the Sixth Assessment Report of the Intergovernmental Panel on Climate Change, pp. 1767-1926, Cambridge University Press, Cambridge, United Kingdom and New York, NY, USA, https://doi.org/10.1017/9781009157896.014, iPCC, chapter 12, 2021.

Rodgers, K. B., Lee, S.-S., Rosenbloom, N., Timmermann, A., Danabasoglu, G., Deser, C., Edwards, J., Kim, J.-E., Simpson, I. R., Stein, K., Stuecker, M. F., Yamaguchi, R., Bódai, T., Chung, E.-S., Huang, L., Kim, W. M., Lamarque, J.-F., Lombardozzi, D. L., Wieder, W. R., and Yeager, S. G.: Ubiquity of human-induced changes in climate variability, Earth System Dynamics, 12, 1393–1411, https://doi.org/10.5194/esd-12-1393-2021, 2021.

Ruehr, S., Keenan, T. F., Williams, C., Zhou, Y., Lu, X., Bastos, A., Canadell, J. G., Prentice, I. C., Sitch, S., and Terrer, C.: Evidence and attribution of the enhanced land carbon sink, Nature Reviews Earth & Environment, 4, 518–534, https://doi.org/10.1038/s43017-023-00456-3, 2023.

Sippel, S., Meinshausen, N., Merrifield, A., Lehner, F., Pendergrass, A. G., Fischer, E., and Knutti, R.: Uncovering the Forced Climate Response from a Single Ensemble Member Using Statistical Learning, Journal of Climate, 32, 5677 – 5699, https://doi.org/10.1175/JCLI-D-18-0882.1, 2019.

Smoliak, B., Wallace, J. M., Lin, P., and Fu, Q.: Dynamical Adjustment of the Northern Hemisphere Surface Air Temperature Field: Methodology and Application to Observations, Journal of climate, 2015.

Swart, N. C., Cole, J. N. S., Kharin, V. V., Lazare, M., Scinocca, J. F., Gillett, N. P., Anstey, J., Arora, V., Christian, J. R., Hanna, S., Jiao, Y., Lee, W. G., Majaess, F., Saenko, O. A., Seiler, C., Seinen, C., Shao, A., Sigmond, M., Solheim, L., von Salzen, K., Yang, D., and Winter, B.: The Canadian Earth System Model version 5 (CanESM5.0.3), Geoscientific Model Development, 12, 4823–4873, https://doi.org/10.5194/gmd-12-4823-2019, 2019.

Walker, A. P., De Kauwe, M. G., Bastos, A., Belmecheri, S., Georgiou, K., Keeling, R. F., McMahon, S. M., Medlyn, B. E., Moore, D. J. P., Norby, R. J., Zaehle, S., Anderson-Teixeira, K. J., Battipaglia, G., Brienen, R. J. W., Cabugao, K. G., Cailleret, M., Campbell, E., Canadell, J. G., Ciais, P., Craig, M. E., Ellsworth, D. S., Farquhar, G. D., Fatichi, S., Fisher, J. B., Frank, D. C., Graven, H., Gu, L., Haverd, V., Heilman, K., Heimann, M., Hungate, B. A., Iversen, C. M., Joos, F., Jiang, M., Keenan, T. F., Knauer, J., Körner, C., Leshyk,

https://doi.org/10.5194/egusphere-2025-1924
Preprint. Discussion started: 19 May 2025
© Author(s) 2025. CC BY 4.0 License.

V. O., Leuzinger, S., Liu, Y., MacBean, N., Malhi, Y., McVicar, T. R., Penuelas, J., Pongratz, J., Powell, A. S., Riutta, T., Sabot, M. E. B., Schleucher, J., Sitch, S., Smith, W. K., Sulman, B., Taylor, B., Terrer, C., Torn, M. S., Treseder, K. K., Trugman, A. T., Trumbore, S. E., van Mantgem, P. J., Voelker, S. L., Whelan, M. E., and Zuidema, P. A.: Integrating the evidence for a terrestrial carbon sink caused by increasing atmospheric CO_2, New Phytologist, 229, 2413–2445, https://doi.org/10.1111/nph.16866, 2021.

Zhang, Y., Ciais, P., Boucher, O., Maignan, F., Bastos, A., Goll, D., Lurton, T., Viovy, N., Bellouin, N., and Li, L.: Disentangling the impacts of anthropogenic aerosols on terrestrial carbon cycle during 1850–2014, Earth's Future, 9, e2021EF002 035, 2021.

Ziehn, T., Chamberlain, M. A., Law, R. M., Lenton, A., Bodman, R. W., Dix, M., Stevens, L., Wang, Y., and Srbinovsky, J.: The Australian Earth System Model: ACCESS-ESM1.5, Journal of Southern Hemisphere Earth Systems Science, 70, 193–214, https://doi.org/10.1071/ES19035, 2020.